ChemComm

COMMUNICATION

View Article Online
View Journal | View Issue

Cite this: *Chem. Commun.*, 2023, 59, 7659

Received 11th April 2023,
Accepted 22nd May 2023

DOI: 10.1039/d3cc01785k

rsc.li/chemcomm

From dots to tubes – the reversed scenario of bottom-up external-catalyst-free synthesis of N-doped carbon nanotubes†

Anna Kolanowska, *[ab] Dariusz Łukowiec, [c] Maciej Krzywiecki, [d] Joanna Bok-Badura [e] and Sławomir Boncel *[af]

We present a novel external-catalyst-free route for the synthesis of N-doped carbon nanotubes (N-CNTs) from amino-acid-derived carbon dots (CDs) as sustainable resources. N-CNTs (~4–26 at% of N) were comprehensively characterized by complementary techniques while the synthetic strategy emerges as an important alternative and, simultaneously, a simply-scalable approach.

Carbon nanotubes (CNTs), with their electronically tunable nitrogen-doped structural variants (N-CNTs), continue to appeal to both scientists and technologists worldwide.[1] This attraction is driven by their 'all-in-one' superb mechanical, electrical, thermal, chemical and biological properties.[2] (N-)CNTs are synthesized mainly *via* arc discharge, laser ablation, and chemical vapor deposition (CVD),[3] while the latter method has emerged as the most scalable route yielding the purest, readily applicable (N-)CNTs.[4] Although this method allows for the synthesis of (N-)CNTs from different carbon sources and in a variety of states of matter, such as gases,[5] liquids[6] or solids,[7] the employment of catalytic amounts of metallic nanoparticles is typically reported as essential for the synthesis of (N-)CNTs.[8]

In 2004, the family of carbon nanoallotropes grew to include carbon dots (CDs) – fluorescent nanomaterials with a carbon core and oxygen/nitrogen functionalities on their surface.[9,10] Those novel and *per se* unique 0D carbon nanomaterials serve as biocompatible fluorescent probes,[11] drug delivery systems,[12] sensors,[13] light emitters,[14] and photocatalysts.[15] One of the top-down methods of CD synthesis is a controlled, fragmentary decomposition of CNTs,[16] or graphite/graphene,[17] whereas bottom-up synthetic methods are based on a progressive polyaromatization and graphitization of low-molecular-weight precursors.[18] And although the synthesis of CNTs and N-CNTs has been studied for more than three decades, the catalyst-free methods were elaborated only for CNTs (with a single report on N-CNTs) (Table S1, ESI†).[19–23] But more importantly, there are no reports on the synthesis of N-CNTs from CDs as a carbon source while, as mentioned above, only the *reverse* scenario was realized.

Here, we report the unique and innovative synthesis and characterization of multi-walled N-CNTs by external-catalyst-free decomposition of amino-acid-derived CDs. Similar to happenstances in the history of carbon nanomaterials, N-CNTs were accidentally discovered in the black deposits – left after thermogravimetric analysis (TGA) of solid amino-acid-derived CDs (displaying from green to blue fluorescence). Our results clearly demonstrate that CDs can be used as structurally tunable and scalable synthetic precursors of N-CNTs.

Firstly, CDs were synthesized from six structurally different natural L-amino acids according to the previously reported protocol (ESI).[18] Next, CDs (10 mg) were placed in an alumina crucible, heated at the 20 °C min^{-1} rate to 800 °C, kept thereat for 3 min, and left to cool down to room temperature – with the total synthesis time of ~1 h in a TGA furnace (TGA 8000, PerkinElmer) (Scheme 1). The whole process was run under a nitrogen flow (20 mL min^{-1}). The highest yield (calculated from the TGA curves describing the synthesis procedure, *i.e.* the percentage ratio of the residual mass and the initial sample weight) of 35% was found for N-CNTs from the His-CDs.

[a] *NanoCarbon Group, Faculty of Chemistry, Department of Organic Chemistry, Bioorganic Chemistry and Biotechnology, Silesian University of Technology, Krzywoustego 4, 44-100 Gliwice, Poland. E-mail: anna.kolanowska@polsl.pl, slawomir.boncel@polsl.pl*
[b] *Biotechnology Centre, Silesian University of Technology, Krzywoustego 8, 44-100 Gliwice, Poland*
[c] *Materials Research Laboratory, Faculty of Mechanical Engineering, Silesian University of Technology, Konarskiego 18A, 44-100 Gliwice, Poland*
[d] *Institute of Physics–CSE, Silesian University of Technology, Konarskiego 22B, 44-100 Gliwice, Poland*
[e] *Faculty of Chemistry, Department of Inorganic, Analytical Chemistry and Electrochemistry, Silesian University of Technology, Krzywoustego 6, 44-100 Gliwice, Poland*
[f] *Centre for Organic and Nanohybrid Electronics (CONE), Silesian University of Technology, Konarskiego 22B, 44-100 Gliwice, Poland*

† Electronic supplementary information (ESI) available. See DOI: https://doi.org/10.1039/d3cc01785k

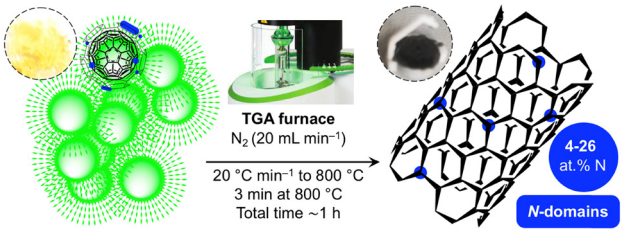

Scheme 1 Scheme of TGA-based amino-acid-CD-N-CNT synthesis; insets show photographs of yellow CDs and a TGA pan with the black N-CNT product.

In parallel, the yield of the Phe-CD-N-CNT product was 18% (Fig. S1, ESI†). The N-CNT yields were ambiguously related to the CD precursor size whereas the highest yields were achieved for CDs with a few-nanometre size. And so, the highest N-CNT yield was achieved for compact His-CDs with a diameter ~1.5 nm; contrarily, for Cys- and Asp-CDs – of a diameter even smaller than 1 nm – the yields of N-CNTs were lower than 10%. This complexity indicates rather the surface and core physicochemistry as the key parameters affecting the yield (Fig. S1, ESI†).

The morphologies and microscopic structure of N-CNTs were characterized by scanning electron microscopy (SEM) (Phenom Pro Desktop SEM, Thermo Fischer Scientific) equipped with an energy-dispersive X-ray spectroscopy (EDX) detector, transmission electron microscopy (TEM) (S/TEM Titan 80–300, 300 kV, Field Electron and Ion Company), TGA (TGA 8000, PerkinElmer), Raman spectroscopy (inVia Confocal Raman microscope, Renishaw, excitation beam wavelength: 633 nm), and X-ray photoelectron spectroscopy (XPS) (PreVac EA15, PreVac). A Varian 710-ES spectrometer equipped with a V-groove nebulizer and a reduced-volume Sturman–Masters type spray chamber was used to determine possible inorganic N-CNT contaminants.

Following the 'from dots to tubes' transformation (Fig. 1), we firstly encounter a TEM image showing a dense agglomerate (due to a sample preparation for the TEM analysis, *i.e.* lyophilized CD samples were re-dispersed in ethanol using an ultrasonic bath) of ~2 nm-wide Phe-CDs containing amorphous shells and semi-graphitic cores (Fig. 1a and Fig. S1, ESI†).[18] TGA synthesis transformed the yellow-orange Phe-CDs into black Phe-CD-N-CNTs of a well-defined, aerogel-like morphology at the macroscale (density 6.7 g dm^{-3}). As shown in the SEM image (Fig. 1b), Phe-CD-N-CNTs were found as flattened, needle-like N-CNT crystallites resembling leaves of a garden plant *Yucca filamentosa* (an inset in Fig. 1b). Furthermore, TEM imaging revealed that the crystallites were composed from the sets of several-micron-long, thick N-CNTs (outer and inner diameters of N-CNTs were found in the range of ~70–90 nm and ~5–10 nm, respectively), with occasionally copresent much thinner, intertwined tubes (again, similarly to threads in *Yucca filamentosa* leaves) (Fig. 1c and d). Only a smaller number (*ca.* 10%) of N-CNTs was found as practically coreless, semi-amorphous fibre-like 1D-objects. The

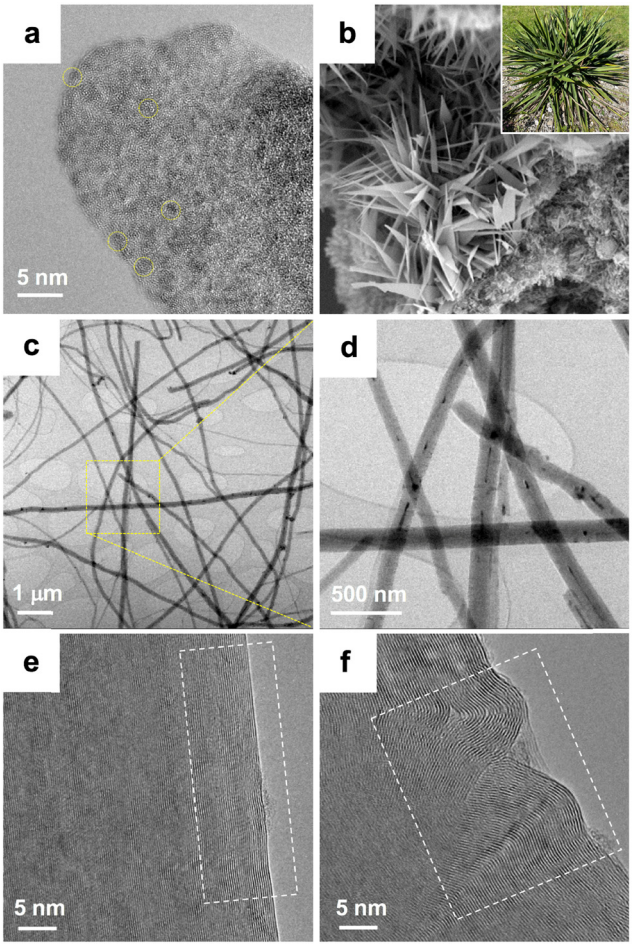

Fig. 1 SEM/TEM imaging of the 'from dots to tubes' transformation: (a) TEM image of the Phe-CD precursor composed of the individual dots – shown by randomly selected circles; (b) SEM image of Phe-CD-N-CNTs crystallites; (c–f) TEM images of Phe-CD-N-CNTs: image (d) represents a magnified area of the (c) image; the most outer layers of N-CNTs showing crystalline, sp^2-carbon-rich (e), and corrugated, wavy-like walls (f).

interlayer spacing in the range of ~0.4 nm resembled that of the only-carbon nanotubes of the multi-wall nature.[24] Indeed, both perfectly crystalline sp^2-carbon-rich (Fig. 1f) and corrugated, wrinkled though well-graphitized (Fig. 1g) domains could be found among the N-CNT walls. Generally, analogous trends were found for all other N-CNTs obtained from CDs synthesized from the other amino-acids (Fig. S2 and S3, ESI†).

TGA curves – acquired under a nitrogen and air atmosphere – for Phe-CDs and the resultant Phe-CD-derived N-CNTs are presented in Fig. 2. Importantly, no significant weight loss up to ~800 °C in N_2 (Fig. 2a) – with the corresponding thermal resistance up to 500 °C in air (Fig. 2b) – was observed only for N-CNTs.

Simultaneously, upon pyrolysis, the derivative thermogravimetry (DTG) analysis showed a single endothermic peak at 696 °C, and at the indicated below temperature for the other amino acids: 758 °C (Lys), 722 °C (His), 687 °C (Gly), and 650 °C (Asp), while uniquely three peaks – at 592, 743, and 801 °C – were found for Cys-CDQ-N-CNTs containing 3.5 ± 0.7 at% of sulphur (Fig. S4a and b, ESI†).

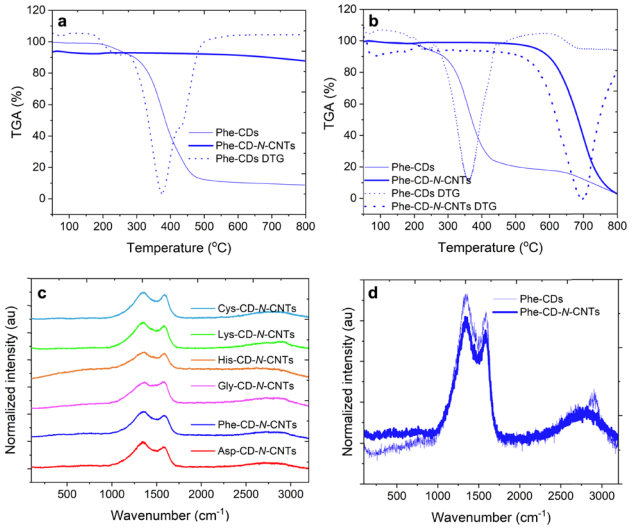

Fig. 2 TGA profiles of the prepared Phe-CDs and Phe-CD-N-CNTs under pyrolytic conditions, *i.e.* a nitrogen atmosphere (with the corresponding DTG for Phe-CDs) (a), TGA and DTG curves of Phe-CDs and Phe-CD-N-CNTs in air (combustion) (b), Raman spectra for all CD-N-CNTs (c), and Raman spectra for Phe-CDs and Phe-CD-N-CNTs (d).

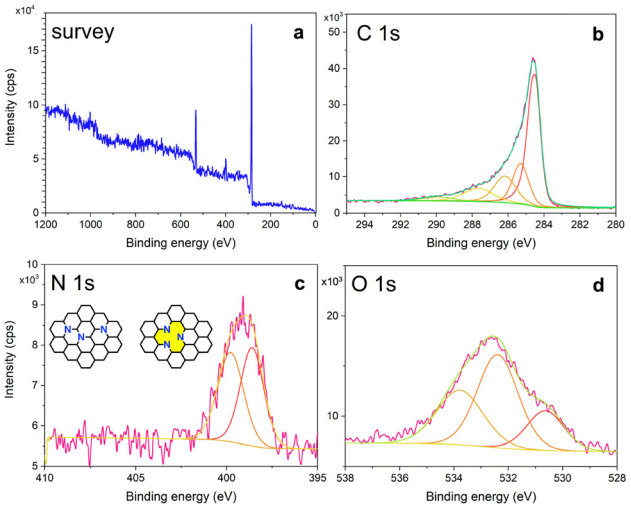

Fig. 3 XPS of Phe-CD-N-CNTs (a), and magnified areas obtained in the C 1s binding energy region (b), N 1s binding energy region (c), and O 1s binding energy region (d); the inset in (c) corresponds to the nearly-equally preferential structural variants of N-doping in the target nanotubes.

Pursuing further the chemical structure of the N-CNTs, we have recorded their Raman spectra (Fig. 2c and d). Indeed, the spectra of all the herein studied N-CNTs showed typical graphitic features: the D-band (a disorder mode) (1345–1369 cm^{-1}) deriving from sp^3-hybridized carbon atoms, the G-band (graphitic mode) (1582–1593 cm^{-1}) arising from the E_{2g} vibration of the graphitic (purely C-sp^2) hybridization, and the second order features corresponding to the 2D-, D + G-, and 2G-combination modes (2780–2897 cm^{-1}).

The relatively high I_D/I_G ratios, *i.e.* 0.99–1.14 (Table S2, ESI†), indicated that the N-CNTs had a comparatively large number of structural defects understood as CNT lattice deformations caused by the presence of both N-sp^3- and N-sp^2-atom-doping scenarios, with a portion of oxygen functionalities.[25] Specifically, for the most crystalline Phe-CD-N-CNT sample (Fig. 2d), the purely C-sp^2 domain displayed, statistically, crystallite sizes as large as ~36 nm (based on the Tuinstra-Koenig relationship) (with ~34 nm for the least crystalline Cys-CD-N-CNT) (Table S2, ESI†).[26]

Fig. 3 shows XPS spectra of Phe-CD-N-CNTs, shown in a full, non-deconvoluted survey version (a), with the main peak of photoemission for C 1s (b). Definitely, the key peak for the C-sp^2 atoms – such as in N-CNTs – could be found at the binding energy (BE) of ~284.5 eV. The peak is broad and bears a long asymmetric tail toward the higher BE values. The C 1s core level was deconvoluted into a few subpeaks located around BE of *ca.* 284 (C–C), 285 (C–O), 286 (C–N), 288 (C═O), and 290 (COOH) eV. In turn, Fig. 3c shows the XPS spectrum in the N 1s BE region, as deconvoluted into the two peaks at 398.5 and 401 eV. Those peaks correspond to the near-equally intensive: (a) gap-generating pyridinic-, and (b) graphitic-like nitrogen atoms, respectively (an inset shows the corresponding structural formulae where the yellow inner space confirms the gap-generating pyridinic-like motifs).[27] Hence, the nitrogen atoms in the N-CNT products occur not only as a part of the functional (as in terminating/tip/gap) groups, but they were successfully incorporated centrally into the N-CNT walls (peak a 398.5 eV after deconvolution of N 1s BE region).[27–29] Indeed, XPS – according to Lazar *et al.*[27] – was recalled as the most powerful spectroscopic method for distinguishing between different N-doping types in graphene as different forms of the nitrogen incorporation have markedly different BEs: the calculated XPS BE of the N 1s state for graphitic and pyridinic in N-CNTs are around 401.5 and 397.9 eV, respectively. Additionally, Fig. 3d shows XPS spectra obtained in the O 1s BE region with the least intense three peaks at 532, 533 and 534 eV. The peak at 533 eV could be assigned to the C–O–C bond, the one at 532 nm to the C═O bonds, while the other at 534 eV could be assigned to –C═O(OH) and ≻C–OH bonds. Analogous relationships were found for N-CNTs obtained from the other amino-acids (Fig. S5–S7, ESI†). Additionally, in order to determine all the inorganic impurities in the exemplary Phe-CD-N-CNT sample, we have performed inductively coupled plasma atomic emission spectrometry (ICP-AES). As a result, seven metallic elements were found above the detection threshold with lead, iron, sodium, and aluminium, as the most significant contaminants present at as low as 10.4, 2.1, 1.8, 1.2 μg mg^{-1} N-CNTs, respectively (Table S3, ESI†). Therefore, a role of the Al_2O_3-pan surface and traces of the above metallic impurities in the possible catalytic activity cannot be fully ruled out. At the same time, the CDs themselves might also be considered as dual in nature, *i.e.* the CDs could serve both as the catalyst and the main carbon/nitrogen source, while their function is rather inseparable. We should also emphasize that we have performed N-CNT synthesis in a laboratory furnace using a quartz tube as the reactor.

Interestingly from the application point-of-view, we have manufactured different electroconductive nanotube coatings (ESI). Phe-CD-N-CNTs emerged as the most conductive 1D fillers in the series of Phe-CD-N-CNTs (surface resistivity of coatings *ca.* 120 Ω sq^{-1}), in-house CVD synthesized ultralong

MWCNTs (d = 60 nm, l = 0.8 mm, *ca.* 250 Ω sq^{-1}), and commercial NC7000™ MWCNTs (d = 10 nm, l = 1.5 μm, *ca.* 100 kΩ sq^{-1}) (Table S4 and Fig. S8, ESI†).

In conclusion, N-CNTs of tunable morphology and surface physicochemistry could be synthesised from amino-acid-derived CDs in a swift, external-catalyst-free procedure. The so obtained N-CNTs had a high I_D/I_G-ratio due to the presence of mainly nitrogen functional groups, thus enabling protocols for novel materials applicable as from-transparent-to-translucent electrodes, multifunctional coatings and self-standing films, or needle-like drug delivery systems, while the above list has now only a rather tentative character. We believe that this new synthetic approach, proceeding in the absence of intentionally introduced metallic nanoparticles and, in fact, excluding the pre-functionalization step, significantly extends the applicability of N-CNTs not only in the field of biomedical materials. For a better understanding of the process of synthesis, a detailed study of the growth mechanisms, and the scaled-up synthesis are currently under investigation.

This work was supported by the National Science Centre PRELUDIUM-18 grant (UMO-2019/35/N/ST5/02563) (A. K.). S. B. is very grateful for the financial support from the National Science Centre (Poland) grant No. 2020/39/B/ST5/02562 in the framework of the OPUS-20 program. S. B. also acknowledges the supporting actions from EU's Horizon 2020 ERA-Chair project ExCEED, grant agreement No. 952008.

Conflicts of interest

There are no conflicts to declare.

References

1 I.-Y. Jeon, H.-J. Noh and J.-B. Baek, *Chem. – Asian J.*, 2020, **15**, 2282–2293.
2 R. Dubey, D. Dutta, A. Sarkar and P. Chattopadhyay, *Nanoscale Adv.*, 2021, **2**, 5722–5744.
3 S. Rathinavel, K. Priyadharshini and D. Panda, *Mater. Sci. Eng. B*, 2021, **268**, 115095.
4 J. H. Ahn, M. N. S. Koo, H. Chan, I. Kim, J. W. Hur, J. H. Lee and J. G. Ok, *Micro Nano Syst. Lett.*, 2019, **7**, 11.
5 G. P. Gakis, S. Termine, A.-F. A. Trompeta, I. G. Aviziotis and C. A. Charitidis, *Chem. Eng. J.*, 2022, **445**, 136807.
6 O. O. Cilsal, M. C. Cakir and A. Uguz, *Surf. Eng.*, 2022, **38**, 472–481.
7 N. A. Fathy and S. El-Shafey, *Int. J. Environ. Sci. Technol.*, 2023, **20**, 293–306.
8 S. Y. Lim and M. M. Norani, *Adv. Mater. Res.*, 2011, **364**, 232–237.
9 X. Xu, R. Ray, Y. Gu, H. J. Ploehn, L. Gearheart, K. Raker and W. A. Scrivens, *J. Am. Chem. Soc.*, 2004, **126**, 12736–12737.
10 P. K. Yadav, S. Chandra, V. Kumar, D. Kumar and S. H. Hasan, *Catalysts*, 2023, **13**, 422.
11 W. Zhang, H. Zhong, P. Zhao, A. Shen, H. Li and X. Liu, *Food Control*, 2022, **133**, 108591.
12 G. Calabrese, G. De Luca, G. Nocito, M. G. Rizzo, S. P. Lombardo, G. Chisari, S. Forte, E. L. Sciuto and S. Conoci, *Int. J. Mol. Sci.*, 2021, **22**, 11783.
13 M. Li, T. Chen, J. J. Gooding and J. Liu, *ACS Sens.*, 2019, **4**, 1732–1748.
14 P. He, Y. Shi, T. Meng, T. Yuan, Y. Li, X. Li, Y. Zhang, L. Fan and S. Yang, *Nanoscale*, 2020, **12**, 4826–4832.
15 Z. W. Heng, W. C. Chong, Y. L. Pang and C. H. Koo, *J. Environ. Chem. Eng.*, 2021, **9**, 105199.
16 J. Zhou, C. Booker, R. Li, X. Zhou, T.-K. Sham, X. Sun and Z. Ding, *J. Am. Chem. Soc.*, 2007, **129**, 744–745.
17 S. Kang, Y. K. Jeong, K. H. Jung, Y. Son, S.-C. Choi, G. S. An, H. Han and K. M. Kim, *RSC Adv.*, 2019, **9**, 38447–38453.
18 A. Kolanowska, G. Dzido, M. Krzywiecki, M. M. Tomczyk, D. Lukowiec, S. Ruczka and S. Boncel, *ACS Omega*, 2022, **7**, 41165–41176.
19 Y. Sun, R. Kitaura, J. Zhang, Y. Miyata and H. Shinohara, *Carbon*, 2014, **68**, 80–86.
20 Z.-Y. Zeng and J.-H. Lin, *RSC Adv.*, 2014, **4**, 40251–40258.
21 S. Huang, Q. Cai, J. Chen, Y. Qian and L. Zhang, *J. Am. Chem. Soc.*, 2009, **131**, 2094–2095.
22 B. Liu, W. Ren, L. Gao, S. Li, S. Pei, C. Liu, C. Jiang and H.-M. Cheng, *J. Am. Chem. Soc.*, 2009, **131**, 2082–2083.
23 X. Xu, S. Huang, Y. Hu, J. Lu and Z. Yang, *Mater. Chem. Phys.*, 2012, **133**, 95–102.
24 K. P. Maity and V. Prasad, *Mater Res. Express*, 2019, **6**, 0850a2.
25 V. D. Blank, E. V. Polyakov, D. V. Batov, B. A. Kulnitskiy, U. Bangert, A. Gutiérrez-Sosa, A. J. Harvey and A. Seepujak, *Diamond Relat. Mater.*, 2003, **12**, 864–869.
26 L. G. Cançado, K. Takai, T. Enoki, M. Endo, Y. A. Kim, H. Mizusaki, A. Jorio, L. N. Coelho, R. Magalhães-Paniago and M. A. Pimenta, *Appl. Phys. Lett.*, 2006, **88**, 163106.
27 P. Lazar, R. Mach and M. Otyepka, *J. Phys. Chem. C*, 2019, **123**, 10695–10702.
28 M. Ayiania, M. Smith, A. J. R. Hensley, L. Scudiero, J.-S. McEwen and M. Garcia-Perez, *Carbon*, 2020, **162**, 528–544.
29 J. D. Bagley, D. K. Kumar, K. A. See and N.-C. Yeh, *RSC Adv.*, 2020, **10**, 39562–39571.

